A Hybrid Mesoscopic/Agent-Based Model for Crowd Dynamics with Emotional Contagion

Aissam Jebrane and Abdelghani El Mousaoui *

Posted Date: 4 December 2025

doi: 10.20944/preprints202512.0466.v1

Keywords: crowd dynamics; hybrid modeling; emotional contagion; kinetic theory; agent-based simulation; emergency evacuation

 doi:10.20944/preprints202512.0466.v1

Article

A Hybrid Mesoscopic/Agent-Based Model for Crowd Dynamics with Emotional Contagion

Aissam Jebrane [1], Abdelghani El Mousaoui [2,*]

[1] Centrale Casablanca, Complex Systems and Interactions Research Center, Ville Verte, Bouskoura 27182, Morocco
[2] Management, Mohammed VI Polytechnic University, Ben Guerir, 43150, Morocco
* Correspondence: abdelghani.elmousaoui@emines.um6p.ma

Abstract

This work investigates crowd dynamics in evacuation scenarios by incorporating the effects of emotional contagion. We develop a hybrid modeling framework that couples a mesoscopic kinetic approach for pedestrian motion with an agent-based model describing emotional interactions. Each individual adapts their emotional state based on the average emotion of nearby agents, which in turn affects their walking direction and speed. Numerical simulations, conducted using a Monte Carlo particle method for the kinetic motion model together with an agent-based scheme for emotional contagion, examine three representative scenarios: calm crowds without contagion, fully emotional crowds, and mixed populations. The results show that emotional contagion intensifies congestion and significantly increases evacuation times. The proposed dual-scale model provides a first step toward a comprehensive representation of panic dynamics, offering new insights into the interplay between motion and emotion, with potential applications to crisis management and safety design.

Keywords: crowd dynamics; hybrid modeling; emotional contagion; kinetic theory; agent-based simulation; emergency evacuation

1. Introduction

Human crowd dynamics play a crucial role in public safety management, particularly during emergency evacuations where individuals must rapidly adapt to stressful and uncertain conditions. As density increases, interactions among pedestrians become highly nonlinear, intertwining physical motion with cognitive and emotional responses. In such situations, emotional contagion can spread rapidly through the population, altering decision-making processes and generating emergent collective patterns that cannot be captured by purely mechanical models. These phenomena underscore the need for advanced mathematical frameworks that integrate both physical displacement and socio-emotional dynamics within a unified multiscale perspective.

Mathematical models of crowd dynamics are commonly categorized into microscopic, mesoscopic, and macroscopic descriptions [1,2]. Microscopic models explicitly track individuals, resolving their positions, velocities, and behavioral states. Classical examples include the Social Force Model (SFM) [3] and Cellular Automata (CA) [4], which have been successfully applied to evacuation dynamics [5] and pedestrian counterflows [6]. These approaches have been further extended to incorporate cognition, mutual influence, and panic effects. For instance, Xu et al. quantified collective disorder in the SFM using mutual information [7], while the ASCRIBE cognitive–emotional framework has been coupled with the SFM to study panic propagation [8]. CA-based models have also been enhanced using game-theoretical rules to represent decision-making and herding behaviors during evacuation [9].

Macroscopic (hydrodynamic) models describe pedestrian motion at the collective scale through conservation laws inspired by fluid mechanics [10]. These models have evolved to include rational path optimization and multiscale interactions [11]. More recently, macroscopic formulations have been

 doi:10.20944/preprints202512.0466.v1

coupled with epidemiological models to explore the interplay between human mobility and disease transmission [12].

Mesoscopic or kinetic models bridge the microscopic and macroscopic scales. In this framework, pedestrians are treated as active particles whose state includes both mechanical variables (e.g., position, velocity) and social variables such as emotional intensity. The overall dynamics are described through a distribution function evolving in time and space over these micro-states. This conceptualization is rooted in the kinetic theory of active particles [13], where living systems are represented as interacting entities endowed with internal variables that influence decision-making and adaptive behavior.

Significant advances in kinetic crowd modeling have been achieved since the pioneering studies by Bellomo et al. [14–16], followed by developments considering interactions with walls, exits, and obstacles in confined environments [17–19]. Behavioral and social components have also been incorporated to investigate emergent collective behaviors and the influence of emotional states on motion patterns [20,21].

A recent review [22] highlights the complexity of human crowds as living systems and identifies key challenges such as multiscale coupling and the integration of rich social dynamics. In this context, general multiscale frameworks have been developed to describe large systems of interacting active entities, incorporating internal variables—such as biological or behavioral states—that modulate interaction rules and drive nonlinear emergent dynamics across scales [23,24]. Following this line of research, a two-dimensional kinetic model for heterogeneous social groups in confined domains was proposed in [25], extending the behavioral framework of [26]. Further contributions examined evacuation processes under infectious disease exposure through unified mesoscopic formulations incorporating behavioral variables [27].

Most kinetic models incorporating emotional or social interactions remain confined to a single mesoscopic scale, where such effects are embedded solely within the distribution function. A few recent works have begun exploring multiscale strategies. In particular, Bellomo et al. [28] proposed a conceptual micro–meso–macro coupling framework, emphasizing the need to connect individual decision-making with emergent macroscopic flow patterns. Other hybrid approaches, such as those developed by Kim et al., inspired by the ASCRIBE framework, couple a microscopic agent-based contagion mechanism with a kinetic model of crowd motion—first in one dimension [29] and later extended to two dimensions [30].

In this work, we propose a hybrid multiscale modeling framework that explicitly couples a continuous mesoscopic kinetic description of pedestrian motion with a microscopic agent-based model governing emotional contagion. Each pedestrian adapts their walking direction through a decision-making process influenced by multiple behavioral drivers: attraction toward the exit, avoidance of obstacles and high-density regions, and aversion to areas of high emotional intensity. Emotional interactions are modeled through a local consensus mechanism, whereby an individual's emotional intensity evolves toward that of neighboring agents. These emotional states, in turn, modulate both the desired walking direction and speed, establishing a bidirectional coupling between motion and emotion. The kinetic component builds upon previous formulations for heterogeneous pedestrian populations [25,26], while the contagion dynamics are inspired by agent-based principles introduced in [31,32]. The resulting multiscale framework provides a coherent and continuous representation of collective motion that naturally integrates socio-emotional influences at the individual level.

Numerical simulations are performed using a Monte Carlo particle method to solve the kinetic displacement model [26,33], while an agent-based simulation tool is employed to model the emotional contagion dynamics [34]. Three representative scenarios are investigated: (i) a calm baseline without contagion, used to validate the kinetic model through fundamental diagrams; (ii) an emotionally responsive crowd, designed to examine how the propagation of emotional intensity impacts evacuation time, pressure, and spatial dispersion; and (iii) heterogeneous populations composed of calm and emotion-susceptible individuals, aimed at evaluating the influence of behavioral diversity. In the present study, the emotional state of each pedestrian is updated according to the average emotional

 doi:10.20944/preprints202512.0466.v1

intensity of their neighbors, providing a first step toward modeling emotional contagion at the mesoscopic level. In future developments, the framework will be extended to account for explicit panic effects and for a broader spectrum of emotional responses—both positive or negative—thereby capturing the full complexity of human affective behavior during crowd evacuations. Moreover, future work may also incorporate the perception of external threats through sensory cues such as auditory alarms or olfactory signals, which play a critical role in triggering emotional and behavioral responses during emergency evacuations [35,36].

The remainder of this paper is organized as follows. Section 2 introduces the mesoscopic kinetic model of pedestrian movement. Section 3 presents the agent-based emotional contagion mechanism and its coupling with the motion dynamics. Section 4 is devoted to numerical simulations and analysis of evacuation dynamics under emotional contagion. Section 5 provides conclusions and discusses future perspectives.

2. Agent Displacement Model

The proposed agent displacement model extends the mesoscopic frameworks developed in [25,26], aiming to describe pedestrian motion within confined environments by accounting for both individual behaviors and emergent collective dynamics.

2.1. Mesoscopic Description

Consider a pedestrian crowd moving within a bounded domain $\Omega \subseteq \mathbb{R}^2$. Each pedestrian, modeled as an active particle, is characterized by a microscopic state defined by their position $\mathbf{x}$ and velocity $\mathbf{v}$. These quantities are expressed in dimensionless form as follows:

- $\mathbf{x} = (x, y)$ denotes the spatial position, normalized with respect to a characteristic length ℓ of the domain Ω.
- $\mathbf{v} \in \mathcal{V} := \{\mathbf{v} : \|\mathbf{v}\| < v_{\lim}\}$, where $v_{\lim}$ represents the maximum walking velocity attainable under free-flow conditions.
- $u \in D_u$ is an activity variable that reflects the behavioral strategy of each pedestrian. For simplicity, u is assumed constant throughout this study.

The crowd is subdivided into n distinct functional subsystems (FSs), each corresponding to a social group or strategy (e.g., pedestrians heading toward a specific exit).

The mesoscopic state of pedestrians belonging to the i-th subsystem is described by the probability density function $f_i = f_i(t, \mathbf{x}, \mathbf{v})$, which defines the distribution of microscopic states at time t:

$$f_i = f_i(t, \mathbf{x}, \mathbf{v}) : [0, T] \times \Omega \times \mathcal{V} \to \mathbb{R}_+, \quad i = 1, \ldots, n,$$

where $f_i(t, \mathbf{x}, \mathbf{v})\, d\mathbf{x}\, d\mathbf{v}$ represents the expected number of pedestrians in subsystem i whose state lies within the infinitesimal phase-space element $[\mathbf{x}, \mathbf{x} + d\mathbf{x}] \times [\mathbf{v}, \mathbf{v} + d\mathbf{v}]$.

Macroscopic quantities can be obtained by taking moments of the distribution function with respect to velocity. The local pedestrian density and mean velocity are defined by:

$$\rho_i(t, \mathbf{x}) = \int_{\mathcal{V}} f_i(t, \mathbf{x}, \mathbf{v})\, d\mathbf{v},$$
$$\boldsymbol{\xi}_i(t, \mathbf{x}) = \frac{1}{\rho_i(t, \mathbf{x})} \int_{\mathcal{V}} \mathbf{v}\, f_i(t, \mathbf{x}, \mathbf{v})\, d\mathbf{v}.$$

Aggregating over all subsystems yields the total density and mean velocity:

$$\rho(t, \mathbf{x}) = \sum_{i=1}^{n} \rho_i(t, \mathbf{x}),$$
$$\boldsymbol{\xi}(t, \mathbf{x}) = \frac{1}{\rho(t, \mathbf{x})} \sum_{i=1}^{n} \rho_i(t, \mathbf{x})\, \boldsymbol{\xi}_i(t, \mathbf{x}).$$

 doi:10.20944/preprints202512.0466.v1

2.2. Derivation of the Mathematical Model

Following the general theory of active particles and stochastic game dynamics [16], we describe the balance of fluxes in the phase space resulting from pedestrian motion and mutual interactions. This balance leads to the following kinetic equation:

$$\begin{aligned}(\partial_t + \mathbf{v}\cdot\nabla_{\mathbf{x}})f_i(t,\mathbf{x},\mathbf{v}) = \eta_A\left(\int_{\mathcal{V}} \mathcal{A}(\mathbf{v}_*\to\mathbf{v})f_i(t,\mathbf{x},\mathbf{v}_*)\,d\mathbf{v}_* - f_i(t,\mathbf{x},\mathbf{v})\right)\\ + \eta_B(\mathbf{x})\left(\int_{\mathcal{V}} \mathcal{B}(\mathbf{v}_*\to\mathbf{v})f_i(t,\mathbf{x},\mathbf{v}_*)\,d\mathbf{v}_* - f_i(t,\mathbf{x},\mathbf{v})\right),\end{aligned} \tag{1}$$

where η_A and η_B denote, respectively, the interaction frequencies between pedestrians and between pedestrians and walls. The transition probability densities $\mathcal{A}$ and $\mathcal{B}$ model the stochastic rules by which pedestrians adapt their velocities due to these interactions. The inter-pedestrian interaction rate η_A is considered uniform across Ω, whereas η_B depends on space, reflecting the increased likelihood of wall interactions near boundaries.

2.3. Modeling Interactions Between Walkers: the $\mathcal{A}$ Term

Interpersonal interactions are a key determinant of collective pedestrian behavior, primarily influencing direction and speed adjustments. The interaction term $\mathcal{A}$, representing these behavioral adaptations, can be factorized into independent components for velocity magnitude and direction:

$$\begin{aligned}\mathcal{A}(\mathbf{v}_*\to\mathbf{v}) &= \mathcal{A}_\theta(\theta_*\to\theta)\,\mathcal{A}_v(v_*\to v),\\ &= \delta(\theta-\theta^{(d)})\,\delta(v-v^{(d)}).\end{aligned}$$

where $v^{(d)}$ and $\theta^{(d)}$ denote the magnitude and direction of the desired velocity in polar coordinates. The corresponding velocity vector is defined as

$$\mathbf{v}^{(d)} = v^{(d)}\,\mathbf{e}^{(d)}, \tag{2}$$

with $\mathbf{e}^{(d)} = (\cos\theta^{(d)}, \sin\theta^{(d)})$ representing the unit vector along the desired direction.

Both $v^{(d)}$ and $\mathbf{e}^{(d)}$ are influenced by the local emotional intensity and are determined according to the behavioral decision rules presented in Section 3.4, which formalize the coupling between motion and emotion.

2.4. Modeling Interactions with Walls: The $\mathcal{B}$ Term

In confined domains, pedestrians adjust their trajectories in anticipation of wall proximity. Following the methodology introduced in [26], we model these nonlocal interactions by assuming that individuals located within a cutoff distance d_w from a wall modify their velocity $\mathbf{v}$ into a new velocity $\mathbf{v}^{(w)}$. This adjustment consists of a linear reduction in the normal velocity component, proportional to the distance d from the wall, while preserving the overall speed. The resulting velocity reads:

$$\mathbf{v}^{(w)} = \frac{d}{d_w}(\mathbf{v}\cdot\mathbf{n})\mathbf{n} + \operatorname{sign}(\mathbf{v}\cdot\mathbf{t})\left[v^2 - \frac{d^2}{d_w^2}(\mathbf{v}\cdot\mathbf{n})^2\right]^{1/2}\mathbf{t}, \tag{3}$$

where $\mathbf{n}$ and $\mathbf{t}$ denote the unit normal and tangential vectors to the wall, respectively. An illustration of this velocity adjustment process is provided in Figure 1.

The associated transition probability density governing wall interactions is expressed as:

$$\mathcal{B}(\mathbf{v}_*\to\mathbf{v}) = \delta(\theta-\theta^{(w)})\,\delta(v-v^{(w)}),$$

where $v^{(w)} = \|\mathbf{v}^{(w)}\|$ and $\theta^{(w)}$ denote the adjusted speed and direction, respectively, determined from Eq. (3). The direction vector is computed as:

 doi:10.20944/preprints202512.0466.v1

$$\frac{\mathbf{v}^{(w)}}{\|\mathbf{v}^{(w)}\|} = (\cos\theta^{(w)}, \sin\theta^{(w)}).$$

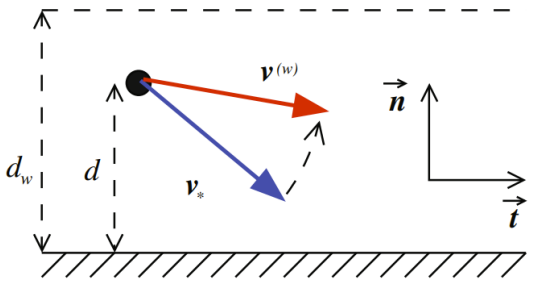

Figure 1. Schematic representation of pedestrian velocity adjustment in the presence of a wall.

3. Emotional Contagion Model

The previous section described the mesoscopic kinetic formulation governing pedestrian displacement. We now focus on the microscopic emotional layer, which captures how emotions spread among individuals and, in turn, influence their motion. This coupling between physical and psychological dynamics is essential for understanding realistic evacuation scenarios, where local emotional interactions can collectively alter global flow patterns.

Emotional dynamics exert a significant influence on crowd behavior, as emotions such as fear, anxiety, or calmness can propagate rapidly through interpersonal interactions. This propagation shapes collective motion, particularly in stressful or emergency situations. To capture these phenomena, we adopt a multi-agent framework inspired by [31,32].

3.1. Microscopic Formulation of Emotional Dynamics

Each pedestrian is modeled as an individual agent located at position x_i and characterized by a time-dependent emotional intensity

$$E_i(t) = E(x_i, t) \in [0,1],$$

where $E_i = 0$ corresponds to a completely calm state and $E_i = 1$ represents maximal emotional activation (e.g., extreme excitement). The emotional state evolves according to the following differential equation:

$$\frac{dE_i}{dt} = \gamma_i\left[\eta_i\left(\beta_i\,\mathrm{PI} + (1-\beta_i)\,\mathrm{NI}\right) + (1-\eta_i)E_i^* - E_i\right], \tag{4}$$

where $\gamma_i > 0$ is the adaptation rate, $\eta_i \in [0,1]$ balances external amplification and social absorption, and E_i^* represents the average emotional state of the neighbors of agent i. Equation (4) integrates three concurrent mechanisms: external stimulation, social contagion, and internal stabilization.

1. **External stimulation:**
$$\gamma_i\,\eta_i\left(\beta_i\,\mathrm{PI} + (1-\beta_i)\,\mathrm{NI}\right),$$
represents the direct effect of external stimuli such as alarms, visible threats, or reassuring signals. The coefficient β_i modulates the sensitivity to positive (PI) versus negative (NI) influences.
2. **Social contagion:** The second term,
$$\gamma_i(1-\eta_i)E_i^*,$$
models the alignment of emotional states through local interactions. The quantity E_i^* is defined as a weighted average of the emotional intensities of neighboring agents:

$$E_i^* = \sum_{j\in\mathcal{N}_i} w_{ji}E_j, \qquad w_{ji} = \frac{\varepsilon_j\alpha_{ji}}{\sum_{k\in\mathcal{N}_i}\varepsilon_k\alpha_{ki}},$$

 doi:10.20944/preprints202512.0466.v1

where ε_j denotes the expressiveness of agent j, α_{ji} measures the strength of the communication channel between j and i, and $\mathcal{N}_i$ represents the neighborhood of i.

3. **Self-regulation:** Finally, the damping term $-\gamma_i E_i$ describes emotional stabilization, ensuring the boundedness of $E_i(t)$ within $[0,1]$ despite fluctuations.

The influence of positive and negative stimuli is quantified as:

$$\mathrm{PI} = 1 - (1 - E_i^*)(1 - E_i), \qquad \mathrm{NI} = E_i^* E_i,$$

which describe, respectively, mutual reassurance and amplification effects.

3.2. Model Parameters and Interpretation

The model parameters define individual heterogeneity and emotional responsiveness:

- **Adaptation rate** γ_i: speed at which agent i reacts to emotional variations;
- **Amplification–absorption balance** η_i: $\eta_i = 1$ corresponds to purely exogenous excitation, while $\eta_i = 0$ represents pure social contagion;
- **Bias coefficient** β_i: controls the relative sensitivity to positive or negative emotional cues.

This microscopic formulation captures a broad range of emotional regimes, from calm cooperative crowds to rapidly destabilized groups under strong contagion effects.

3.3. Pure Absorption Regime

In the present study, we restrict attention to the *pure absorption* regime ($\eta_i = 0$), in which no external emotional amplification is considered. Equation (4) then simplifies to:

$$\frac{dE_i}{dt} = \gamma_i \left(E_i^* - E_i\right), \tag{5}$$

where each individual tends to align their emotional intensity with the local average of their neighbors, leading asymptotically to a collective emotional consensus. Here, the local average E_i^* is defined as:

$$E_i^* = \sum_{j \in \mathcal{N}_i} w_{ji} E_j, \qquad w_{ji} = \frac{\varepsilon_j \alpha_{ji}}{\sum_{k \in \mathcal{N}_i} \varepsilon_k \alpha_{ki}}.$$

To obtain a tractable mesoscopic representation, we first consider a simplified configuration in which individuals adapt their emotional intensity to the mean emotional state of surrounding agents. This assumption is formalized through the following hypotheses:

(H1) **Homogeneous interaction strength:** communication weights are assumed to be locally uniform, i.e., $\alpha_{ji} \approx \bar{\alpha}$ and $\varepsilon_j \approx \bar{\varepsilon}$ within the neighborhood of agent i;

(H2) **Symmetric and isotropic interactions:** emotional influence is considered symmetric among neighbors, so that each neighboring agent contributes equally to the perceived emotional field;

(H3) **Continuum approximation:** the discrete set of neighbors $\mathcal{N}_i$ is replaced by a local density of agents distributed around the position x_i.

Under these assumptions, the normalized weights w_{ji} become uniform,

$$w_{ji} \approx \frac{1}{|\mathcal{N}_i|},$$

which yields the simplified form of the local emotional average:

$$E_i^* = \frac{1}{|\mathcal{N}_i|} \sum_{j \in \mathcal{N}_i} E_j.$$

 doi:10.20944/preprints202512.0466.v1

This continuous field $E^*(x,t)$ will later be used to modify the potential governing pedestrian motion, thereby coupling emotional contagion with collective displacement dynamics.

3.4. Coupling Between Emotion and Motion

Pedestrian motion is governed not only by physical constraints and spatial organization but also by emotional and cognitive factors that modulate perception and decision-making under stress.

In this work, we propose a unified formulation in which the *desired direction of motion* derives from a total potential function $\Phi(x,t)$, representing the perceived cost or discomfort associated with each spatial location. This potential combines a *mechanical reference component*, accounting for environmental and density-related effects, with an *emotional component*, reflecting the collective affective state of the crowd.

Pedestrian decision-making is assumed to result from the superposition of several behavioral drives, described as follows:

(A1) **Attraction toward exits:** individuals are motivated to move toward the nearest exit, minimizing the distance to safety;
(A2) **Avoidance of obstacles and congestion:** pedestrians tend to favor regions of lower density to preserve comfort and avoid physical contact;
(A3) **Aversion to emotionally intense zones:** highly stressed areas are perceived as undesirable, generating a repulsive influence on motion.

The behavioral assumptions (A1)–(A3) provide the foundation upon which the potential fields are constructed and parameterized in the following formulation.

The total potential is decomposed as:

$$\Phi(x,t) = \Phi_{\text{ref}}(x,t) + \Delta\Phi(x,t), \tag{6}$$

where:

- $\Phi_{\text{ref}}(x,t)$ is the **mechanical reference potential**, representing the baseline tendency to approach exits and avoid congestion;
- $\Delta\Phi(x,t)$ is the **emotional potential**, capturing the influence of collective affective states on pedestrian motion.

The reference potential reflects spatial and physical constraints that dominate under calm conditions:

$$\Phi_{\text{ref}}(x,t) = w_d D(x) + w_\rho \rho(x,t),$$

where $D(x)$ denotes the geodesic distance to the nearest exit, $\rho(x,t)$ is the local pedestrian density, and $w_d, w_\rho > 0$ are weighting parameters tuning the relative importance of evacuation urgency and comfort. This term corresponds to the so-called "calm-class" behavior, describing pedestrian motion in non-stressful environments.

The originality of the present formulation lies in the introduction of an emotional potential that couples the collective emotional field to pedestrian dynamics:

$$\Delta\Phi(x,t) = w_E E^*(x,t),$$

where $E^*(x,t)$ denotes the local mean emotional intensity, and $w_E > 0$ measures its influence on decision-making. An increase in $E^*(x,t)$ elevates the perceived discomfort of a region, thereby acting as a repulsive potential that diverts pedestrians from highly stressed or dangerous zones.

The total potential thus becomes:

$$\Phi(x,t) = w_d D(x) + w_\rho \rho(x,t) + w_E E^*(x,t),$$

 doi:10.20944/preprints202512.0466.v1

providing a compact yet interpretable representation of the coupling between physical and psychological influences in crowd motion.

The desired velocity of a pedestrian located at position x and time t, as defined in the displacement model by equation (2), is expressed as:

$$\mathbf{v}^{(d)}(x,t) = v^{(d)}(x,t)\,\mathbf{e}^{(d)}(x,t), \tag{7}$$

where the desired direction $\mathbf{e}^{(d)}(x,t)$ is oriented along the steepest descent of the total potential, normalized to unit length:

$$\mathbf{e}^{(d)}(x,t) = -\frac{\nabla\Phi(x,t)}{\|\nabla\Phi(x,t)\|}.$$

Hence, pedestrians naturally tend to move in the direction of decreasing potential, corresponding to regions of lower perceived discomfort.

In addition to direction, emotional states also influence walking speed $v^{(d)}(x,t)$. The variation of walking speed depends on local interactions among pedestrians. More precisely, individuals continuously adjust their velocity magnitude in response to environmental conditions, local congestion, and their own emotional state relative to that of nearby agents. In this study, the dependence of speed on local density is grounded in the fundamental diagram of pedestrian flow [37], further extended to incorporate emotional effects through a modulation function $\sigma(E(x,t))$ that captures the influence of emotional intensity on motion.

In the absence of emotional modulation, the desired speed is typically expressed as a monotonically decreasing function of the perceived local density $\rho_p(x,t)$. Following the classical exponential formulation of the fundamental diagram, we define the desired speed as:

$$v^{(d)}(x,t) = v_M\left\{1 - \exp\left[-\zeta\left(\frac{1}{\rho_p(x,t)} - \frac{1}{\rho_M}\right)\right]\right\} \cdot \sigma(E(x,t)), \tag{8}$$

where v_M denotes the free (maximum) walking speed, ρ_M the jam (maximum) density, $\rho_p(x,t)$ the perceived local density, and $\zeta > 0$ an empirical shape parameter fitted from experimental or observational data [38]. This density-dependent relation reproduces the well-known decrease in pedestrian speed with increasing congestion.

The function $\sigma(E(x,t))$ introduces the modulation induced by emotional interactions. It reflects the tendency of individuals to adjust their pace according to the emotional intensity of both themselves and their neighbors. A smooth logistic formulation is adopted:

$$\sigma(E(x,t)) = \frac{1}{1 + \exp\left[\kappa\big(E(x,t) - E^*(x,t)\big)\right]}, \tag{9}$$

where $E^*(x,t)$ denotes the local average emotional intensity defined as

$$E_i^* = \frac{1}{|\mathcal{N}_i|}\sum_{j\in\mathcal{N}_i} E_j,$$

and $\kappa > 0$ controls the sharpness of the behavioral transition.

This formulation ensures a smooth and adaptive modulation of walking speed:

- If $E(x,t) \approx E^*(x,t)$, the pedestrian's emotional state matches the local environment, and the walking speed remains close to the nominal desired value ($\sigma \approx 1$);
- If $E(x,t) > E^*(x,t)$, the individual exhibits a higher emotional activation than the surrounding crowd, which may lead to hesitation or uncoordinated movements, thus reducing the effective speed;
- If $E(x,t) < E^*(x,t)$, the individual is calmer than the local average, and the modulation slightly increases their effective speed to adapt to the surrounding flow.

 doi:10.20944/preprints202512.0466.v1

The proposed coupling mechanism constitutes the link between emotional contagion dynamics and the motion model within a potential-based framework. This formulation consistently integrates psychological and physical influences into a unified mathematical structure. The emotional field modulates both the direction (via Φ) and the magnitude (via $\sigma(E(x,t))$) of motion, enabling emergent behaviors such as the avoidance of emotionally charged zones and self-organized rerouting. This coupling bridges micro-level emotional interactions and macro-level evacuation patterns, providing a foundation for more realistic and predictive simulations of collective dynamics in emergency scenarios.

4. Numerical Experiments

This section presents the simulation framework and numerical results aimed at evaluating the impact of emotional dynamics and the mobility laws defined in our model. The experiments are designed to isolate and quantify the effects of density and emotional contagion on collective pedestrian behavior. More specifically, the numerical campaign addresses two main objectives: (i) comparing the reference case of a calm crowd with that of an emotional crowd, and (ii) providing a first extension toward heterogeneous populations, paving the way for future developments, including the explicit integration of panic phenomena.

4.1. Numerical Methodology

The coupled kinetic–agent model is solved using a hybrid Monte Carlo strategy that combines a Direct Simulation Monte Carlo (DSMC) [33] approach for the kinetic transport equation with an explicit agent-based scheme for the emotional contagion dynamics.

We consider the kinetic equation over a spatial domain $\Omega \subset \mathbb{R}^2$ and a velocity domain $\mathcal{V} \subset \mathbb{R}^2$, on a time interval $[0,T]$:

$$\begin{cases} (\partial_t + \mathbf{v}\cdot\nabla_{\mathbf{x}})f(t,\mathbf{x},\mathbf{v}) = \eta_A\Big(\displaystyle\int_{\mathcal{V}} \mathcal{A}(\mathbf{v}_*\to\mathbf{v})f(t,\mathbf{x},\mathbf{v}_*)\,d\mathbf{v}_* - f(t,\mathbf{x},\mathbf{v})\Big) \\ \qquad + \eta_B(\mathbf{x})\Big(\displaystyle\int_{\mathcal{V}} \mathcal{B}(\mathbf{v}_*\to\mathbf{v})f(t,\mathbf{x},\mathbf{v}_*)\,d\mathbf{v}_* - f(t,\mathbf{x},\mathbf{v})\Big), \\ f(0,\mathbf{x},\mathbf{v}) = f_0(\mathbf{x},\mathbf{v}), \qquad \mathbf{x}\in\Omega,\ \mathbf{v}\in\mathcal{V}. \end{cases} \tag{10}$$

Here, η_A and $\eta_B(\mathbf{x})$ denote the interaction frequencies associated with pedestrian–pedestrian and pedestrian–wall interactions, respectively. The transition kernels $\mathcal{A}$ and $\mathcal{B}$ encode stochastic velocity updates toward the desired direction $\mathbf{v}^{(d)}$ and wall-reflected velocity $\mathbf{v}^{(w)}$.

4.1.1. Splitting Strategy

To solve the kinetic problem efficiently, we employ an operator-splitting approach that separates the distinct physical mechanisms acting on pedestrians. This decomposition allows each process—interaction, boundary reflection, and free transport—to be treated independently within each time step.

We discretize the time interval $[0,T]$ into steps

$$t_0, t_1, \ldots, t_{N_T}, \quad \text{with } t_{n+1} - t_n = \Delta t,$$

assuming a uniform time step Δt for simplicity. Within each interval $[t^n, t^{n+1}]$, the solution is advanced as:

$$f^{n+1} = P_C^{\Delta t} P_B^{\Delta t} P_A^{\Delta t} f^n, \tag{11}$$

where

- $P_A^{\Delta t}$ represents *inter-pedestrian interactions*,
- $P_B^{\Delta t}$ accounts for *wall reflections and boundary effects*,

 doi:10.20944/preprints202512.0466.v1

- $P_C^{\Delta t}$ corresponds to the *free transport* of pedestrians.

Thus, the solution evolves sequentially as

$$f^n \xrightarrow{P_A^{\Delta t}} f_A^{n+1} \xrightarrow{P_B^{\Delta t}} f_B^{n+1} \xrightarrow{P_C^{\Delta t}} f^{n+1}.$$

The first two operators are treated stochastically using a Monte Carlo approach, while $P_C^{\Delta t}$ is computed deterministically by particle advection.

(i) Inter-pedestrian interactions $(P_A^{\Delta t})$.

$$\begin{cases} \partial_t f = \eta_A \Big(\int_{\mathcal{V}} \mathcal{A}(\mathbf{v}_* \to \mathbf{v}) f(\mathbf{x}, \mathbf{v}_*)\, d\mathbf{v}_* - f(\mathbf{x}, \mathbf{v}) \Big), \\ f(0, \mathbf{x}, \mathbf{v}) = f^n(\mathbf{x}, \mathbf{v}). \end{cases} \tag{12}$$

This term models the local adaptation of velocity due to mutual interactions. Each pedestrian tends to align its motion with a desired direction $\mathbf{e}^{(d)}$ and speed $v^{(d)}$, both influenced by cognitive and emotional factors. The interaction kernel $\mathcal{A}$ is modeled as a Dirac delta centered at the desired velocity:

$$\mathcal{A}(\mathbf{v}_* \to \mathbf{v}) = \delta(\mathbf{v} - \mathbf{v}^{(d)}), \qquad \mathbf{v}^{(d)} = v^{(d)} \mathbf{e}^{(d)} = v^{(d)} (\cos\theta^{(d)}, \sin\theta^{(d)})$$

(ii) Wall interactions $(P_B^{\Delta t})$.

$$\begin{cases} \partial_t f = \eta_B(\mathbf{x}) \Big(\int_{\mathcal{V}} \mathcal{B}(\mathbf{v}_* \to \mathbf{v}) f(\mathbf{x}, \mathbf{v}_*)\, d\mathbf{v}_* - f(\mathbf{x}, \mathbf{v}) \Big), \\ f(0, \mathbf{x}, \mathbf{v}) = f_A^{n+1}(\mathbf{x}, \mathbf{v}). \end{cases} \tag{13}$$

The kernel $\mathcal{B}$ is a Dirac delta centered at the reflected velocity $\mathbf{v}^{(w)}$, determined by the wall rule (3). Numerically, when a particle approaches a wall ($d_w < d_{\text{th}}$), its velocity is replaced by $\mathbf{v}^{(w)}$.

(iii) Free transport $(P_C^{\Delta t})$.

$$\begin{cases} \partial_t f + \mathbf{v} \cdot \nabla_{\mathbf{x}} f = 0, \\ f(0, \mathbf{x}, \mathbf{v}) = f_B^{n+1}(\mathbf{x}, \mathbf{v}), \end{cases} \tag{14}$$

whose analytical solution is

$$f(\mathbf{x}, \mathbf{v}, t + \Delta t) = f_B^{n+1}(\mathbf{x} - \mathbf{v}\Delta t, \mathbf{v}, t),$$

so that each particle moves linearly as

$$\mathbf{x}_p^{n+1} = \mathbf{x}_p^n + \mathbf{v}_p^n \Delta t.$$

4.1.2. Agent-Based Emotional Contagion Scheme

Emotional contagion is modeled through an explicit agent-based update derived from Eq. (5). For each particle i:

$$E_i^{n+1} = E_i^n + \Delta t\, \gamma_i (E_i^* - E_i^n), \qquad E_i^* = \frac{1}{|\mathcal{N}_i|} \sum_{j \in \mathcal{N}_i} E_j^n, \tag{15}$$

where $\mathcal{N}_i$ denotes the set of neighbors within perception radius R_p. This averaging mechanism drives local emotional alignment, while the relaxation coefficient γ_i controls the rate of convergence. The updated emotion E_i^{n+1} influences the desired speed and orientation through the modulation function $\sigma(E)$ and the decision potential $\Phi(\mathbf{x}, t)$.

 doi:10.20944/preprints202512.0466.v1

4.1.3. Monte Carlo Resolution of Inter-Pedestrian Interactions $P_A^{\Delta t}$

Applying a forward Euler discretization to (12) yields

$$f^{n+1}(\mathbf{x},\mathbf{v}) = (1-\eta_A\Delta t)\, f^n(\mathbf{x},\mathbf{v}) + \eta_A\Delta t \int_{\mathcal{V}} \mathcal{A}(\mathbf{v}_*\to\mathbf{v})\, f^n(\mathbf{x},\mathbf{v}_*)\, d\mathbf{v}_*. \tag{16}$$

Substituting $\mathcal{A}(\mathbf{v}_*\to\mathbf{v}) = \delta(\mathbf{v}-\mathbf{v}^{(d)})$ gives

$$\int_{\mathcal{V}} \mathcal{A}(\mathbf{v}_*\to\mathbf{v}^d)\, f^n(\mathbf{x},\mathbf{v}_*)\, d\mathbf{v}_* = \rho^n(\mathbf{x})\,\delta(\mathbf{v}-\mathbf{v}^{(d)}), \quad \rho^n(\mathbf{x}) = \int_{\mathcal{V}} f^n(\mathbf{x},\mathbf{v}_*)\, d\mathbf{v}_*.$$

Hence, the updated distribution reads:

$$f^{n+1}(\mathbf{x},\mathbf{v}) = (1-\eta_A\Delta t)\, f^n(\mathbf{x},\mathbf{v}) + \eta_A\Delta t\,\rho^n(\mathbf{x})\,\delta(\mathbf{v}-\mathbf{v}^{(d)}), \tag{17}$$

which preserves the local density $\rho^n(\mathbf{x})$.

If f^n is normalized as a probability density, then $\rho^n(\mathbf{x})$ is replaced by 1 in (17), yielding

$$f^{n+1} = (1-\eta_A\Delta t)\, f^n + \eta_A\Delta t\,\delta(\mathbf{v}-\mathbf{v}^{(d)}),$$

Under the condition $\eta_A\Delta t \le 1$, f^{n+1} is thus a convex combination of two probability densities.

This admits the following probabilistic interpretation at the particle level: at each time step, each particle updates its velocity according to

- With probability $1-\eta_A\Delta t$, the particle retains its current velocity: $\mathbf{v}_p^{n+1} = \mathbf{v}_p^n$.
- With probability $\eta_A\Delta t$, the particle adopts the desired velocity: $\mathbf{v}_p^{n+1} = \mathbf{v}^{(d)}$.

The desired direction is obtained from the decision potential Φ and the desired speed combines density effects and emotional modulation:

$$\begin{aligned} \mathbf{e}^{(d)}(\mathbf{x},t) &= -\frac{\nabla\Phi(\mathbf{x},t)}{\|\nabla\Phi(\mathbf{x},t)\|}, \qquad \Phi(\mathbf{x},t) = w_d D(\mathbf{x}) + w_\rho \rho(\mathbf{x},t) + w_E E^*(\mathbf{x},t), \\ v^{(d)}(\mathbf{x},t) &= v_M\left[1-\exp\left(-\zeta\left(\frac{1}{\rho_p}-\frac{1}{\rho_M}\right)\right)\right]\sigma(E(\mathbf{x},t)), \qquad \sigma(E) = \frac{1}{1+\exp[\kappa(E-E_{\text{crit}})]}. \end{aligned} \tag{18}$$

where D is the distance-to-exit potential, ρ the perceived local density, and E^* the averaged emotional field.

Let $\{(\mathbf{x}_p^n, \mathbf{v}_p^n, E_p^n)\}_{p=1}^N$ denote the simulated particle time t^n. The stochastic update of $P_A^{\Delta t}$ proceeds as follows:

Algorithm 1: Nanbu-like Monte Carlo algorithm for $P_A^{\Delta t}$

for $p = 1,\dots,N$ **do**

1. Compute desired direction $\mathbf{e}^{(d)}(\mathbf{x}_p^n, t^n) = -\nabla\Phi/\|\nabla\Phi\|$ and desired speed $v^{(d)}$.
2. Set desired velocity $\mathbf{v}_p^{(d)} = v^{(d)}(E_p^{n+1})\mathbf{e}^{(d)}(\mathbf{x}_p^n, t^n)$;
3. Update velocity probabilistically:
   - With probability $1-\eta_A\Delta t$, keep the current velocity: $\mathbf{v}_p^{n+1} = \mathbf{v}_p^n$;
   - With probability $\eta_A\Delta t$, adopt the desired velocity: $\mathbf{v}_p^{n+1} = \mathbf{v}_p^{(d)}$.

The full hybrid algorithm advancing the solution from t^n to $t^{n+1} = t^n + \Delta t$ combines emotional contagion dynamics with stochastic inter-pedestrian and wall interactions, as well as deterministic free transport. Each time step consists of the operations described in Algorithm 2.

 doi:10.20944/preprints202512.0466.v1

Algorithm 2: Complete Monte Carlo–Agent Coupled Time Step

for $n = 0, \ldots, N_T - 1$ **do**

Step 1. Emotional contagion update.

for $p = 1, \ldots, N$ **do**

$$E_p^{n+1} = E_p^n + \Delta t\, \gamma_p \big(E_p^* - E_p^n\big), \quad E_p^* = \frac{1}{|\mathcal{N}_p|} \sum_{j \in \mathcal{N}_p} E_j^n.$$

This step models local emotional alignment within perception radius R_p.

Step 2. Compute decision potential and desired direction.

Evaluate the potential field and direction at each particle position:

$$\Phi(\mathbf{x}_p^n, t^n) = w_d D(\mathbf{x}_p^n) + w_\rho \rho(\mathbf{x}_p^n, t^n) + w_E E^*(\mathbf{x}_p^n, t^n), \qquad \mathbf{e}^{(d)}(\mathbf{x}_p^n, t^n) = -\frac{\nabla \Phi}{\|\nabla \Phi\|}.$$

Step 3. Compute desired velocity.

The desired speed is determined by perceived density ρ_p and emotion E_p^{n+1}:

$$v_p^{(d)} = v_M \Big[1 - \exp\Big(-\zeta\Big(\tfrac{1}{\rho_p} - \tfrac{1}{\rho_M}\Big)\Big)\Big] \sigma(E_p^{n+1}), \quad \sigma(E) = \frac{1}{1 + \exp[\kappa(E - E_{\text{crit}})]},$$

and the desired velocity is $\mathbf{v}_p^{(d)} = v_p^{(d)}\, \mathbf{e}^{(d)}(\mathbf{x}_p^n, t^n)$.

Step 4. Inter-pedestrian interaction step ($P_A^{\Delta t}$).

Each particle updates its velocity stochastically according to:

- With probability $1 - \eta_A \Delta t$, keep the current velocity: $\mathbf{v}_p^{n+1} = \mathbf{v}_p^n$;
- With probability $\eta_A \Delta t$, adopt the desired velocity: $\mathbf{v}_p^{n+1} = \mathbf{v}_p^{(d)}$.

Step 5. Wall reflection step ($P_B^{\Delta t}$).

For each particle close to a wall ($d_w(\mathbf{x}_p^n) < d_{\text{th}}$), apply the stochastic reflection rule:

- With probability $1 - \eta_B(\mathbf{x}_p^n)\Delta t$, keep the velocity: $\mathbf{v}_p^{n+1} = \mathbf{v}_p^{n+1}$;
- With probability $\eta_B(\mathbf{x}_p^n)\Delta t$, adopt the reflected velocity:

$$\mathbf{v}_p^{n+1} = \mathbf{v}_p^{(w)} = \mathbf{v}_p^{n+1} - 2\big(\mathbf{v}_p^{n+1} \cdot \mathbf{n}_w(\mathbf{x}_p^n)\big)\, \mathbf{n}_w(\mathbf{x}_p^n).$$

Step 6. Free transport step ($P_C^{\Delta t}$).

Each particle moves deterministically according to its current velocity:

$$\mathbf{x}_p^{n+1} = \mathbf{x}_p^n + \mathbf{v}_p^{n+1} \Delta t.$$

Step 7. Reconstruction of macroscopic fields: $\rho(\mathbf{x}, t^{n+1}), E^*(\mathbf{x}, t^{n+1}), \rho_p$.

This splitting-based hybrid scheme preserves local mass, ensures probabilistic consistency of velocity updates, and naturally couples emotional, cognitive, and physical dynamics in a unified Monte Carlo framework.

4.2. Simulation Strategy

We adopt a two-step complementary simulation strategy:

- **Calm crowds (reference case without emotion):** In the first step, we consider crowds composed exclusively of agents from the calm class, without accounting for emotional contagion. This configuration allows us to validate the mobility model against the fundamental speed–density relation and to compute the following baseline indicators:

 doi:10.20944/preprints202512.0466.v1

  - Fundamental diagram (speed–density relation),
  - Average pedestrian flow,
  - Average kinetic pressure,
  - Average kinetic dispersion,
  - Mean evacuation time.
- **Crowds with emotional contagion:** In the second step, emotional dynamics and contagion are introduced into the population. This setup enables us to analyze how individual and collective emotional intensity modifies pedestrian trajectories, speeds, and evacuation efficiency. The comparison with the calm case highlights the effect of emotional reactivity and its modulation of speed and direction.
- **Heterogeneous crowds (calm + emotional contagion):** Finally, we investigate mixed scenarios where a fraction p of agents is subject to contagion, while the remaining agents remain calm. The objectives are to identify:
  - the impact of the fraction p on evacuation performance,
  - the possible existence of critical thresholds beyond which contagion significantly disrupts collective dynamics.

4.3. Simulation Scenario and Parameters

The evacuation scenario is inspired by a section of the platform at Casablanca Voyageurs station (Morocco). The computational domain is a rectangular area of 20 m in length and 5 m in width, featuring a single 2 m wide exit located along the lower boundary.

Initially, 45 agents are uniformly distributed within a 10 m $\times$ 2 m region centered in the domain, yielding an initial density of $\rho = 2.25 \text{ped}/\text{m}^2$.

The simulations rely on the following physical and emotional parameters:

- Maximum walking speed: $v_M = v_{\text{lim}} = 2$ m/s,
- Reference density: $\rho_M = 7 \text{ped}/\text{m}^2$,
- Emotional influence radius (for contagion effects): $R = 2$ m,
- Adaptation rate: $\gamma_i \sim \mathcal{U}(0,1)$.

Figure 2 presents snapshots of the agent density at successive time instants for the calm scenario.

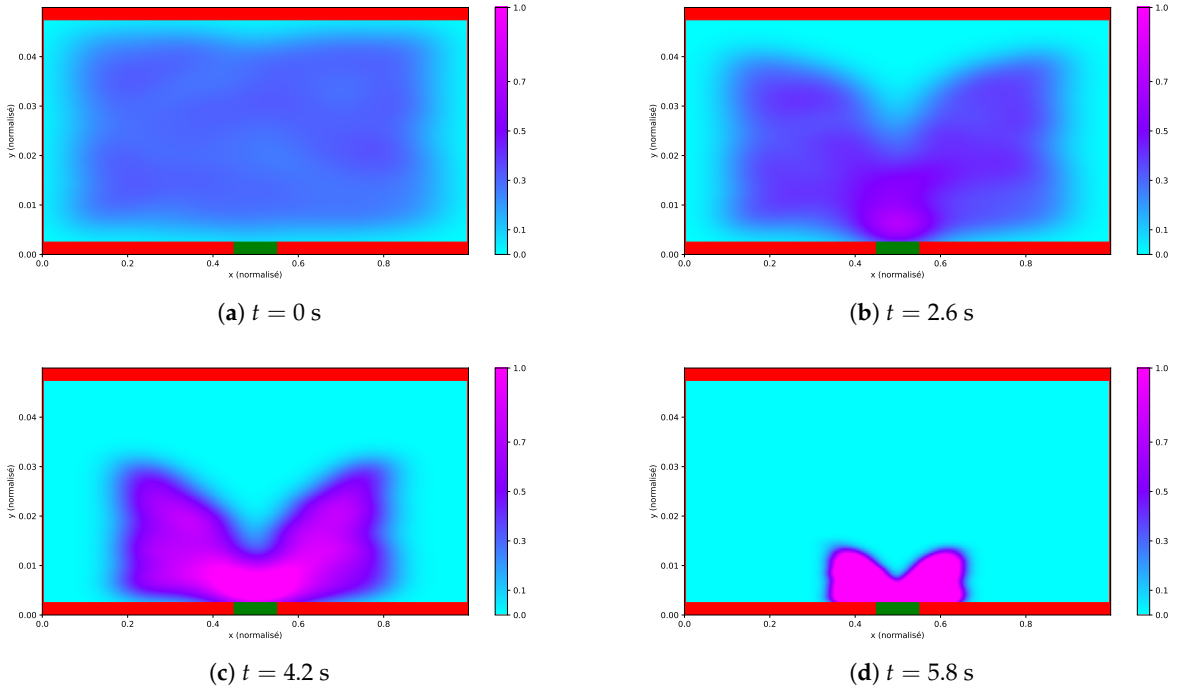

(**a**) $t = 0$ s (**b**) $t = 2.6$ s

(**c**) $t = 4.2$ s (**d**) $t = 5.8$ s

Figure 2. Density plots of a calm crowd at different times: (a) $t = 0$ s, (b) $t = 2.6$ s, (c) $t = 4.2$ s, and (d) $t = 5.8$ s.

 doi:10.20944/preprints202512.0466.v1

These results provide a qualitative validation of the kinetic model through its consistency with the fundamental speed-density relationship, and they establish a baseline for comparison with simulations incorporating emotional contagion.

4.4. Quantitative Indicators

To evaluate the simulations, we compute a set of kinetic and emotional indicators characterizing both microscopic and macroscopic features of the evacuation dynamics.

1. Fundamental diagram (speed–density relation).

As a first validation step, the model is tested against the classical relation between walking speed and density. The average speed is measured as a function of the average density and compared with the Kladek–Weidmann formulation [37].

2. Average pedestrian flow.

The pedestrian flow at position x and time t is defined as

$$q(t,x) = \rho(t,x)\,\xi(t,x),$$

where $\rho(t,x)$ is the local density and $\xi(t,x)$ the mean velocity.

3. Local kinetic pressure.

The kinetic pressure quantifies the fluctuation of individual velocities around the local mean velocity:

$$P(t,x) = \int_{\mathbb{R}^2} \|v - \xi(t,x)\|^2 f(t,x,v)\,dv,$$

where $f(t,x,v)$ is the distribution function and $\xi(t,x)$ the mean velocity:

$$\xi(t,x) = \frac{1}{\rho(t,x)} \int_{\mathbb{R}^2} v f(t,x,v)\,dv, \qquad \rho(t,x) = \int_{\mathbb{R}^2} f(t,x,v)\,dv.$$

Kinetic pressure therefore measures the local agitation of pedestrians around their collective motion.

4. Local kinetic dispersion.

The dispersion, or velocity variance, is defined by:

$$\mathrm{Disp}(t,x) = \frac{1}{\rho(t,x)} \int_{\mathbb{R}^2} \|v - \xi(t,x)\|^2 f(t,x,v)\,dv,$$

which is directly related to the kinetic pressure by:

$$\mathrm{Disp}(t,x) = \frac{P(t,x)}{\rho(t,x)}.$$

It provides a normalized measure of velocity fluctuations, independent of density, and is thus suitable to quantify heterogeneity of motion.

5. Evacuation time.

The global evacuation time T_{evac} is defined as the earliest instant when the domain is effectively empty:

$$T_{\mathrm{evac}} = \inf\{t > 0 \mid \|\rho(t,\cdot)\|_{L^1} \approx 0\}.$$

 doi:10.20944/preprints202512.0466.v1

6. Average emotional intensity.

The emotional intensity of individual i at time t is denoted by $E_i(t)$. The population-wide average is defined as:

$$\overline{E}(t) = \frac{1}{N} \sum_{i=1}^{N} E_i(t),$$

which provides a macroscopic measure of the collective emotional state. Its temporal evolution highlights how contagion modulates group behavior during evacuation.

4.5. Numerical Results and Analysis

4.5.1. Numerical Results and Discussion for a Calm Crowd Scenario

In this first scenario, the population consists exclusively of calm agents, without any emotional contagion. The objective is to validate the proposed kinetic mobility model under neutral behavioural conditions and to establish a baseline for subsequent scenarios involving emotional dynamics. To this end, five quantitative indicators are evaluated—namely the speed–density relation, the flow–density curve, the evacuation time, the kinetic pressure, and the kinetic dispersion—as summarised in Figure 3.

Fundamental diagram (speed–density relation).

The relationship between mean walking speed and density exhibits the expected monotonic decrease (Figure 3A). At low densities, pedestrians move near their desired velocity, whereas higher densities induce progressive slowdowns due to increased interactions. This behaviour aligns with classical empirical laws and confirms that the kinetic formulation captures fundamental pedestrian-flow properties [37].

Average pedestrian flow.

The flow–density curve displays the typical concave profile (Figure 3B). Flow increases with density until reaching a peak around $\rho \approx 2$ ped/m^2, after which congestion reduces throughput. The maximum flow, approximately 0.45 ped·m^{-1}·s^{-1}, is consistent with empirical benchmarks reported for unidirectional motion [39].

Evacuation time.

The evacuation time increases nonlinearly with the initial density (Figure 3C). For densities below 2 ped/m^2, clearance is rapid (less than 3 s), while higher densities yield a sharp escalation, with evacuation times exceeding 10 s for $\rho > 5$ ped/m^2. This reflects the onset of near-jamming conditions and the associated decline in collective mobility.

Local kinetic pressure and dispersion.

Kinetic pressure and microscopic dispersion quantify velocity fluctuations and local disorder (Figure 3D,E). Both remain low during free-flow phases but increase significantly near the exit where density accumulates. A pronounced dispersion peak appears around $t \approx 1000$ iterations, corresponding to the most congested phase, before decreasing as the domain clears. These trends provide complementary insight into the internal stability of the crowd in the absence of emotional effects.

The results for the calm crowd validate the kinetic model against well-established pedestrian dynamics laws. All indicators exhibit consistent and physically meaningful behavior. The walking speed decreases progressively with increasing density, while the pedestrian flow reaches its maximum at intermediate density levels before declining under congestion. The global evacuation time shows a nonlinear growth pattern as density rises, highlighting the increasing difficulty of collective motion near jamming conditions. Moreover, the local amplification of velocity fluctuations—reflected in the pressure and dispersion fields—reveals intensified interactions at bottlenecks. Overall, these outcomes confirm that the kinetic formulation successfully reproduces classical collective dynamics

 doi:10.20944/preprints202512.0466.v1

in the absence of emotional factors, thus providing a robust baseline for evaluating the influence of emotional contagion in subsequent simulations.

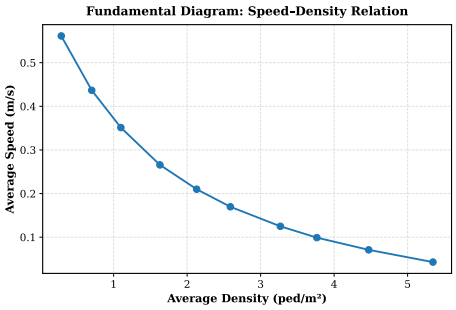

(A) Fundamental diagram.

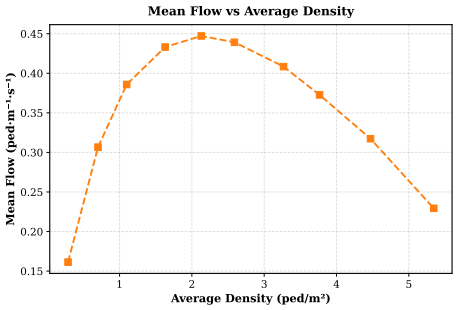

(B) Flow–density relation.

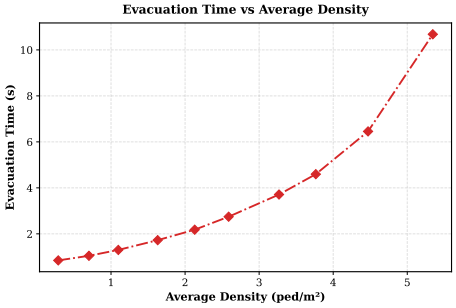

(C) Evacuation time.

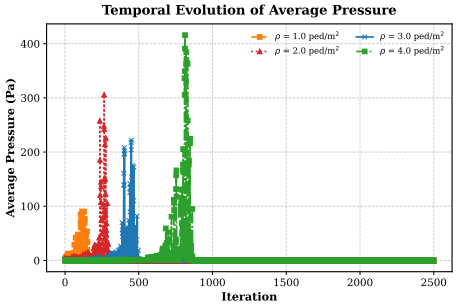

(D) Kinetic pressure evolution.

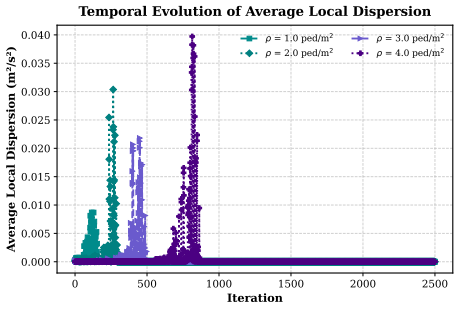

(E) Kinetic dispersion evolution.

Figure 3. Numerical indicators for a calm crowd: (A) fundamental diagram, (B) flow–density relation, (C) evacuation time, (D) kinetic pressure evolution, (E) kinetic dispersion evolution.

4.5.2. Effects of Emotional Contagion on Crowd Dynamics

We simulate evacuation scenarios in which emotional states propagate among pedestrians, and compare the results to a calm (non-reactive) baseline. Figure 4 illustrates six key metrics capturing how contagion alters collective motion. In each case, emotional stress amplifies the usual density-dependent trends.

The fundamental diagram (speed–density relation) predicts that walking speed decreases as density increases [40,41]. With emotional contagion, this decline becomes more pronounced: for a given density, the mean speed remains consistently lower than in the calm configuration. As shown in Figure 4(A), this reduction stems solely from the coupling between emotional intensity, desired velocity, and decision potentials.

 doi:10.20944/preprints202512.0466.v1

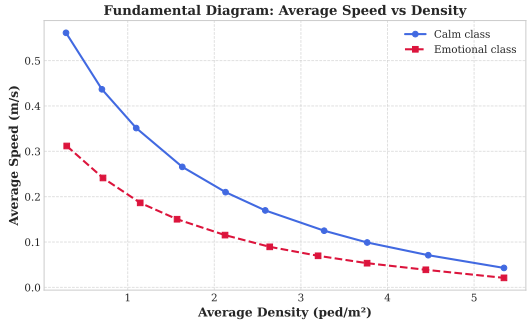

(A) Fundamental diagram: average speed vs density.

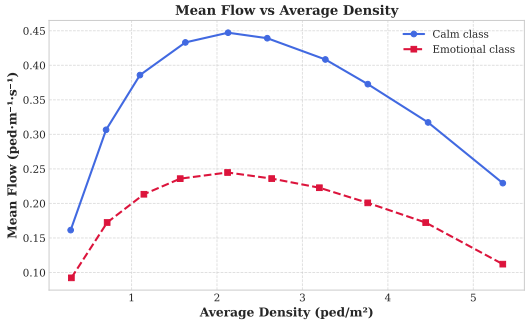

(B) Pedestrian flow as a function of density.

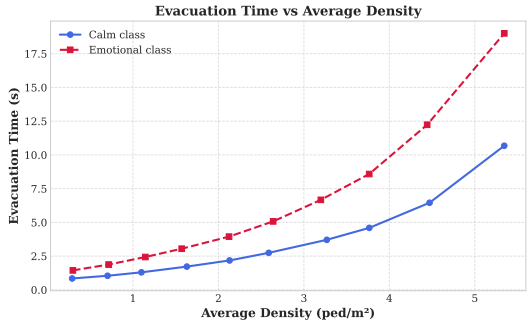

(C) Global evacuation time vs density.

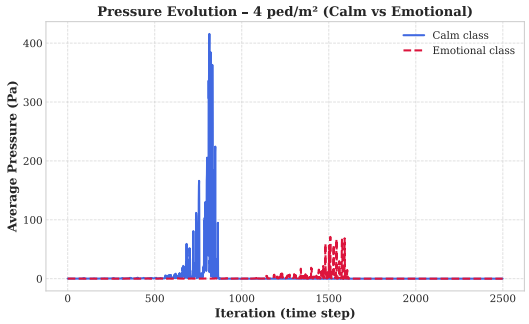

(D) Evolution of local kinetic pressure.

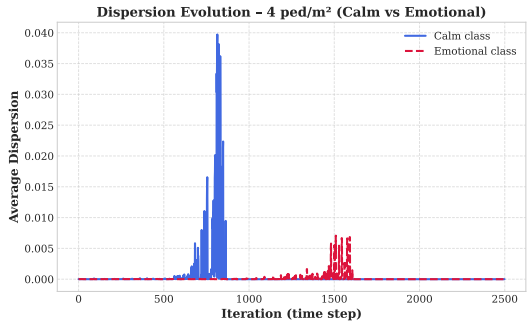

(E) Average local dispersion vs time.

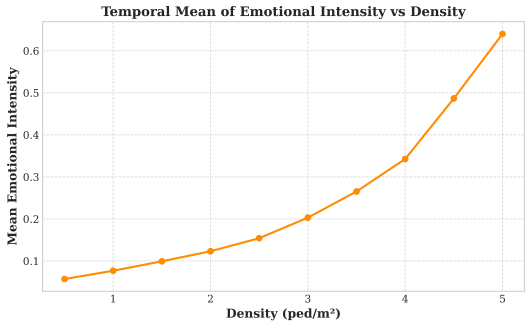

(F) Temporal evolution of average emotional intensity.

Figure 4. Impact of emotional contagion on crowd dynamics: (A) fundamental diagram, (B) pedestrian flow, (C) evacuation time, (D) kinetic pressure, (E) dispersion, (F) emotional intensity.

A similar effect appears in the flow–density relationship (Figure 4(B)). The maximum flow decreases and congestion occurs at lower densities. This behaviour reflects the reduced coordination induced by emotional alignment, which modifies local decision-making and leads to less efficient collective motion. Although qualitatively compatible with studies incorporating emotional factors [42, 43], the present dynamics result exclusively from the simplified mean-contagion mechanism used here.

Consequently, the evacuation time increases for all initial densities (Figure 4(C)). Emotional contagion alters interaction patterns and decision outcomes, which slows down global motion. Similar trends have been reported in models that include internal-state or emotion-related variables [44].

The spatial distribution of kinetic pressure (Figure 4(D)) also exhibits higher and more heterogeneous peaks when contagion is active. This behaviour should be interpreted as a mechanical consequence of decreased coordination rather than as an indicator of physical competition. Comparable pressure patterns have been observed in interaction-based models [45].

 doi:10.20944/preprints202512.0466.v1

The dispersion (Figure 4(E)) also increases, indicating more irregular local trajectories. This emerges from fluctuations in emotional intensity and their influence on directional choices.

Finally, the average emotional intensity (Figure 4(F)) increases during congestion phases and decreases as pedestrians exit the domain. This trend is consistent with the mean-contagion formulation: higher densities produce stronger interaction rates, leading to faster emotional alignment. Similar density–emotion feedbacks appear in other contagion-based frameworks [32]. In summary, the six indicators collectively show the impact of emotional contagion on evacuation dynamics:

- steeper decrease in walking speed with density,
- reduced maximal flow and earlier transition to congestion,
- longer evacuation times,
- higher kinetic pressure and greater trajectory dispersion,
- increased emotional intensity during high-density phases.

Overall, these results demonstrate that even a minimal emotional-contagion mechanism can significantly influence emergent evacuation behaviour. Emotional alignment modifies desired velocities and local decision processes, reducing coordination and flow efficiency. The proposed framework therefore provides a first step toward more detailed modelling of emotional influences or panic-related phenomena in future work.

4.5.3. Impact of Emotional Proportion on Heterogeneous Crowd Dynamics

In this scenario, the crowd is composed of a mixture of calm and emotional agents. The proportion of emotional individuals p varies from 0% to 100%, allowing a systematic assessment of how emotional contagion influences both global evacuation performance and local dynamic indicators. This configuration represents a realistic situation where only part of the population initially reacts to an emotional stimulus, while the rest remains calm or progressively adapts through social interaction.

(A) Fundamental diagram — Speed versus density.

Figure 5(A) shows the average pedestrian speed as a function of density for various emotional proportions. For all cases, the average speed decreases monotonically with increasing density, confirming the expected congestion effect. However, as p increases, the overall velocity levels drop significantly. In particular, a fully emotional crowd ($p = 1$) exhibits the lowest mobility due to stronger avoidance interactions and increased hesitation, whereas the calm case ($p = 0$) maintains smoother and faster movement. This clearly indicates that emotional activation negatively impacts local coordination and mobility.

(B) Flow–density relation.

The corresponding flow–density relation is presented in Figure 5(B). For each emotional proportion, the flux first increases with density, reaches a maximum (the capacity point), and then decreases due to congestion. As the proportion p rises, both the peak flow and the optimal density shift downward, showing that emotional contagion reduces the efficiency of collective movement and triggers earlier saturation. This behavior reflects a degradation of cooperative motion and an enhancement of self-interaction among emotional agents.

(C) Evacuation efficiency.

Figure 5(C) depicts the total evacuation time as a function of the emotional proportion for a fixed density ($\rho = 2.0$ ped/m^2). The evacuation time increases almost linearly with p, indicating that even a moderate fraction of emotional individuals can significantly slow down the evacuation. This is mainly caused by the amplification of local blockages and hesitation zones induced by emotional feedback, which decrease the global outflow rate.

Preprints.org (www.preprints.org) | NOT PEER-REVIEWED | Posted: 4 December 2025 doi:10.20944/preprints202512.0466.v1

(D) Emotional indicators.

Finally, Figure 5(D) shows the evolution of the average emotional intensity and the fraction of panicked agents with respect to p. The mean emotional level increases nearly linearly, confirming the collective amplification of emotions through contagion mechanisms. Nevertheless, the fraction of panicked agents remains small, meaning that while emotions propagate widely, only a limited subset of agents reaches the panic threshold. This demonstrates the model's capability to capture graded emotional responses rather than binary panic transitions.

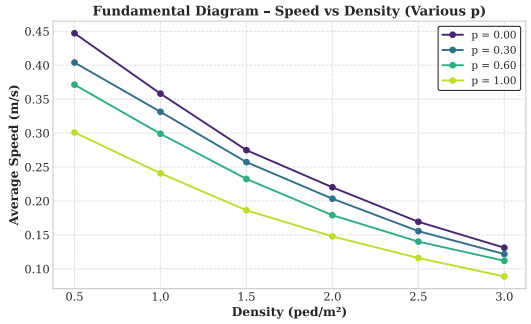

(A) Fundamental diagram for different emotional proportions.

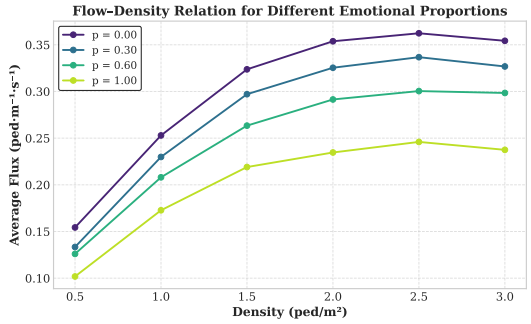

(B) Flow rate as a function of density.

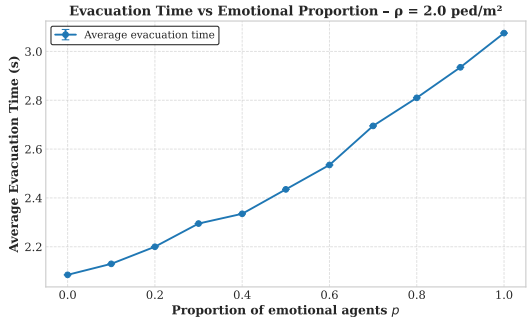

(C) Total evacuation time vs emotional proportion.

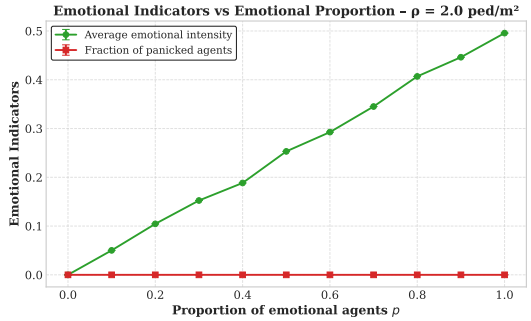

(D) Mean emotional intensity evolution.

Figure 5. Influence of the proportion of emotional agents on evacuation dynamics: (A) fundamental diagram, (B) pedestrian flow, (C) evacuation time, (D) mean emotional intensity.

Overall, these results highlight the substantial impact of emotional heterogeneity on evacuation dynamics. As the proportion of emotional agents increases, the crowd exhibits lower average speeds, reduced flow efficiency, and longer evacuation times. The interplay between density effects and emotional contagion provides a plausible explanation for the deterioration of evacuation performance observed in realistic high-stress scenarios.

5. Conclusion and Future Perspectives

This work presented a hybrid kinetic–agent modelling framework for crowd evacuation dynamics that integrates emotional contagion, decision-based motion, and stochastic interaction operators. On the modelling side, the approach combines a mesoscopic kinetic description of pedestrian motion with an agent-based formulation of emotional interactions, enabling a unified representation of physical movement, cognitive decisions, and affective influences.

On the numerical side, coupling a Nanbu-like Monte Carlo scheme with the agent-level contagion mechanism allows the simulations to capture the nonlinear interplay between interactions, decision making, and emotions. The results show that emotional activation plays a decisive role in shaping evacuation performance: increasing the proportion of emotionally affected individuals reduces flow efficiency, accelerates congestion, and disrupts coordinated motion, as reflected in the fundamental di-

 doi:10.20944/preprints202512.0466.v1

agrams, evacuation times, and emotional intensity fields. These observations highlight the importance of incorporating emotional feedback when modelling crowd behaviour under stress.

It is worth emphasizing that the present study focuses exclusively on mean emotional contagion, whereby each agent aligns its emotional intensity with the local average of its neighbours. This simplified formulation was deliberately adopted to isolate and quantify the influence of emotions on evacuation efficiency. Within this controlled setting, we were able to assess how emotional amplification alters decision potentials, desired velocities, and ultimately the collective dynamics. As such, this work should be viewed as a foundational step toward more detailed modelling of panic phenomena in emergency scenarios.

Several natural perspectives arise from this first level of emotional modelling. A key direction concerns polarity-dependent contagion, in which calming, neutral, and destabilizing emotions propagate differently. Recent studies using modified social-force and agent-based models have demonstrated that personality traits modulate panic spread, and that moderate levels of emotional arousal can improve evacuation efficiency, whereas excessive panic can significantly reduce coordination and flow performance [46]. Introducing polarity-dependent contagion would enable competitive contagion patterns and richer collective behaviours than the simple averaging scheme adopted here.

Another promising avenue involves adaptive decision strategies, where individuals adjust the weights of their decision potential according to local density, perceived threat, or evolving emotional cues. Data-driven kinetic models have recently been proposed to infer stress levels in real time and dynamically adjust agent decision-making parameters [47–49]. In addition, agent-based studies indicate that competitive agents can imitate cooperative behaviours according to the social context, profoundly influencing evacuation dynamics [49].

Beyond these extensions, it is also relevant to situate this work within broader developments in kinetic modelling of social systems. In particular, the evolutionary artificial-world framework proposed by Bellomo and Egidi [50] provides a conceptual foundation for modelling heterogeneous populations whose interaction rules evolve over time. Incorporating such ideas into the present kinetic–agent structure would allow emotions, decision mechanisms, and interaction patterns to co-evolve dynamically, thus bridging the gap between static contagion rules and more realistic, adaptive behavioural dynamics.

Additional extensions include the study of complex geometries, multimodal interactions, dynamic visibility conditions, as well as theoretical analysis of the kinetic operators. For instance, recent kinetic models introduce "awareness" states that influence agent movement and decision-making, offering a pathway to extend the framework to more realistic geometrical and environmental scenarios [51]. Finally, data-driven calibration of emotional parameters represents a crucial direction: multi-source contagion models, including those developed in social media contexts, demonstrate the value of calibrating emotional dynamics from heterogeneous input channels, which could improve the realism of crowd simulations [52].

Overall, the proposed framework establishes a mathematically consistent basis for coupling emotions, interactions, and decision making in evacuation modelling. While intentionally restricted to mean emotional alignment, this study provides a solid foundation for developing more advanced descriptions of panic emergence and heterogeneous behavioural responses in future work.

References

1. Cristiani, E.; Piccoli, B.; Tosin, A. *Multiscale Modeling of Pedestrian Dynamics*; Springer International Publishing: Berlin, 2014.
2. Bellomo, N.; Dogbe, C. On the modeling of traffic and crowds: A survey of models, speculations, and perspectives. *SIAM Review* **2011**, *53*, 409–463.
3. Helbing, D.; Molnár, P. Social force model for pedestrian dynamics. *Physical Review E* **1995**, *51*, 4282.
4. Kirchner, A.; Schadschneider, A. Simulation of evacuation processes using a bionics-inspired cellular automaton model for pedestrian dynamics. *Physica A* **2002**, *312*, 260–276.

 doi:10.20944/preprints202512.0466.v1

5. Yang, X.; Hairong, D.; Qianling, W.; Yao, C.; Xiaoming, H. Guided crowd dynamics via modified social force model. *Physica A* **2014**, *411*, 63–73.
6. Corbetta, A.; Meeusen, J.; Lee, C.M.; Benzi, R.; Toschi, F. Physics-based modeling and data representation of pairwise interactions among pedestrians. *Physical Review E* **2018**, *98*, 062310.
7. Xu, M.; Wang, Y.; Li, P.; Jiang, H.; Li, M.; Ye, Y. miSFM: on combination of mutual information and social force model towards simulating crowd evacuation. *Neurocomputing* **2015**, *168*, 529–537.
8. Lamrhary, Y.; Jebrane, A.; Argoul, P.; Boukamel, A.; Hakim, A. A Coupled SFM-ASCRIBE Model to Investigate the Influence of Emotions and Collective Behavior in Homogeneous and Heterogeneous Crowds. *Collective Dynamics* **2024**, *9*, 1–29.
9. Zheng, X.; Cheng, Y. Conflict game in evacuation process: A study combining Cellular Automata model. *Physica A* **2011**, *390*, 1042–1050.
10. Henderson, L.F. The statistics of crowd fluids. *Nature*, *229*, 1971.
11. Cristiani, E.; Priuli, F.; Tosin, A. Modeling rationality to control self-organization of crowds: An environmental approach. *SIAM Journal on Applied Mathematics* **2015**, *75*, 605–629.
12. Salam, A.; Shamim, P.; Wolfgang, B.; Axel, K.; Sudarshan, T. Disease contagion models coupled to crowd motion and mesh-free simulation. *Mathematical Models and Methods in Applied Sciences* **2021**, *31*, 1277–1295.
13. Bellomo, N.; Burini, D.; Dosi, G.; Gibelli, L.; Knopoff, D.; Outada, N.; Virgillito, M.E. What is life? A perspective of the mathematical kinetic theory of active particles. *Mathematical Models and Methods in Applied Sciences* **2021**, *31*, 1821–1866.
14. Bellomo, N.; Bellouquid, A. On the modeling of crowd dynamics: Looking at the beautiful shapes of swarms. *Networks and Heterogeneous Media* **2011**, *6*, 383–399.
15. Bellomo, N.; Bellouquid, A.; Knopoff, D. From the microscale to collective crowd dynamics. *Multiscale Modeling & Simulation* **2013**, *11*, 943–963.
16. Bellomo, N.; Knopoff, D.; Soler, J. On the difficult interplay between life, complexity, and mathematical sciences. *Mathematical Models and Methods in Applied Sciences* **2013**, *23*, 1861–1913.
17. Agnelli, J.; Colasuonno, F.; Knopoff, D. A kinetic theory approach to the dynamics of crowd evacuation from bounded domains. *Mathematical Models and Methods in Applied Sciences* **2015**, *25*, 109–129.
18. Elmoussaoui, A.; Argoul, P.; Rhabi, M.E.; Hakim, A. Discrete kinetic theory for 2D modeling of a moving crowd: Application to the evacuation of a non-connected bounded domain. *Computers & Mathematics with Applications* **2018**, *75*, 1159–1180.
19. Kim, D.; Quaini, A. A kinetic theory approach to model pedestrian dynamics in bounded domains with obstacles. *Kinetic and Related Models* **2019**, *12*, 1273–1296.
20. Bellomo, N.; Gibelli, L. Toward a mathematical theory of behavioral-social dynamics for pedestrian crowds. *Mathematical Models and Methods in Applied Sciences* **2015**, *25*, 2417–2437.
21. Bellomo, N.; Gibelli, L.; Outada, N. On the interplay between behavioral dynamics and social interactions in human crowds. *Kinetic and Related Models* **2019**, *12*, 397–409.
22. Bellomo, N.; Liao, J.; Quaini, A.; Russo, L.; Siettos, C. Human behavioral crowds: Review, critical analysis, and research perspectives. *Mathematical Models and Methods in Applied Sciences* **2023**, *33*, 1611–1659.
23. Bellomo, N.; Bingham, R.; Chaplain, M.A.; Dosi, G.; Forni, G.; Knopoff, D.A.; Lowengrub, J.; Twarock, R.; Virgillito, M.E. A multiscale model of virus pandemic: Heterogeneous interactive entities in a globally connected world. *Mathematical Models and Methods in Applied Sciences* **2020**, *30*, 1591–1651.
24. Bellomo, N.; Ha, S.Y.; Outada, N.; Yoon, J. On the mathematical theory of behavioral swarms emerging collective dynamics. *Mathematical Models and Methods in Applied Sciences* **2022**, *32*, 2927–2959.
25. Bakhdil, N.; Mousaoui, A.E.; Hakim, A. A kinetic theory approach to model pedestrian social groups behavior in bounded domain. *Kinetic and Related Models* **2024**, *17*, 88–106.
26. Bellomo, N.; Gibelli, L. Behavioral crowds: Modeling and Monte Carlo simulations toward validation. *Computers & Fluids* **2016**, *141*, 13–21.
27. Agnelli, J.; Buffa, B.; Knopoff, D.; Torres, G. A spatial kinetic model of crowd evacuation dynamics with infectious disease contagion. *Bulletin of Mathematical Biology* **2023**, *85*, 23.
28. Bellomo, N.; Gibelli, L.; Quaini, A.; Reali, A. Towards a mathematical theory of behavioral human crowds. *Mathematical Models and Methods in Applied Sciences* **2022**, *32*, 321–358.
29. Kim, D.; Quaini, A. Coupling kinetic theory approaches for pedestrian dynamics and disease contagion in a confined environment. *Mathematical Models and Methods in Applied Sciences* **2020**, *30*, 1893–1915.
30. Kim, D.; O'Connell, K.; Ott, W.; Quaini, A. A kinetic theory approach for 2D crowd dynamics with emotional contagion. *Mathematical Models and Methods in Applied Sciences* **2021**, *31*, 1137–1162.

 doi:10.20944/preprints202512.0466.v1

31. Bosse, T.; Duell, R.; Memon, Z. Agent-Based Modeling of Emotion Contagion in Groups. *Cognitive Computation* **2015**, *7*, 111–136.
32. Durupinar, F.; Pelechano, N.; Allbeck, J. Investigating the effect of personality on communication and emotion contagion in crowds. *Computer Animation and Virtual Worlds* **2016**, *27*, 311–320.
33. Pareschi, L.; Toscani, G. *Interacting multiagent systems: kinetic equations and Monte Carlo methods*; OUP Oxford, 2013.
34. Haeringen, E.S.V.; Gerritsen, C.; Hindriks, K.V. Emotion contagion in agent-based simulations of crowds: a systematic review. *Autonomous Agents and Multi-Agent Systems* **2023**, *37*, 6.
35. Zeng, J.; Rebelo, F.; He, R.; Noriega, P.; Vilar, E.; Wang, Z. Using virtual reality to explore the effect of multimodal alarms on human emergency evacuation behaviors. *Virtual Reality* **2025**, *29*, 1–15.
36. Khan, H.; Nilsson, D. Smell of fire increases behavioural realism in virtual reality: A case study on a recreated MGM Grand hotel fire. In Proceedings of the 2023 IEEE International Symposium on Mixed and Augmented Reality (ISMAR). IEEE, 2023, pp. 820–828.
37. Bruno, L.; Tosin, A.; Tricerri, P.; Venuti, F. Non-local first-order modelling of crowd dynamics: A multidimensional framework with applications. *Applied Mathematical Modelling* **2011**, *35*, 426–445.
38. Fruin, J.J. *Pedestrian planning and design*; Elevator World Inc., 1987.
39. Zhang, J.; Klingsch, W.; Schadschneider, A.; Seyfried, A. Ordering in bidirectional pedestrian flows and its influence on the fundamentaldiagram. *Journal of Statistical Mechanics: Theory and Experiment* **2012**, *2012*, P02002.
40. Helbing, D.; Farkas, I.; Vicsek, T. Simulating dynamical features of escape panic. *Nature* **2000**, *407*, 487–490.
41. Hoogendoorn, S.; Bovy, P. Pedestrian route-choice and activity scheduling theory and models. *Transportation Research Part B* **2004**, *38*, 169–190.
42. Parisi, D.; Dorso, C. Microscopic dynamics of pedestrian evacuation. *Physica A* **2005**, *354*, 606–618.
43. Johansson, A.; Helbing, D.; Shukla, P. Specification of the social force pedestrian model by evolutionary adjustment to video tracking data. *Advances in Complex Systems* **2007**, *10*, 271–288.
44. Cao, M.; Zhang, G.; Wang, M.; Lu, D.; Liu, H. A method of emotion contagion for crowd evacuation. *Physica A: Statistical Mechanics and its Applications* **2017**, *483*, 250–258.
45. Zheng, X.; Zhong, T.; Liu, M. Modeling crowd evacuation of a building based on seven methodological approaches. *Building and Environment* **2009**, *44*, 437–445.
46. Ren, J.; Mao, Z.; Gong, M.; Zuo, S. Modified social force model considering emotional contagion for crowd evacuation simulation. *International Journal of Disaster Risk Reduction* **2023**, *96*, 103902.
47. Kim, D.; Labate, D.; Mily, K.; Quaini, A. Data driven learning to enhance a kinetic model of distressed crowd dynamics. *arXiv preprint arXiv:2411.12974* **2024**.
48. Templeton, A.; Xie, H.; Gwynne, S.; Hunt, A.; Thompson, P.; Köster, G. Agent-based models of social behaviour and communication in evacuations: A systematic review. *Safety Science* **2024**, *176*, 106520.
49. Zablotsky, A.; Kuperman, M.; Bouzat, S. Pedestrian evacuations with imitation of cooperative behavior. *Physical Review E* **2024**, *109*, 054304.
50. Bellomo, N.; Egidi, M. From Herbert A. Simon's legacy to the evolutionary artificial world with heterogeneous collective behaviors. *Mathematical Models and Methods in Applied Sciences* **2024**, *34*, 145–180.
51. Agnelli, J.P.; Armas, C.; Knopoff, D. Spatial Kinetic Modeling of Crowd Evacuation: Coupling Social Behavior and Infectious Disease Contagion. *Symmetry* **2025**, *17*, 123.
52. Chen, H.; Jiamin, J.; Sun, S.; Zhang, C.; Yu, M. Research on propagation dynamics of emotional contagion using S3EIR model based on multiple social media platforms. *Frontiers in Communication* **2025**, *10*, 1582974.